

GPS/IMU Error Analysis for Airborne SAR Remote Sensing

L.J. Harcke, R.M. Ueberschaer, J.W. Sinko, and J.M. Strus
SRI International

BIOGRAPHY

Leif J. Harcke joined SRI International in 2004 as a senior research engineer in the area of imaging radar systems engineering. He received the B.S. and M.Eng. degrees from Cornell University and the Ph.D. degree from Stanford University, all in the field of electrical engineering. Before joining SRI he was a member of the technical staff at the Jet Propulsion Laboratory.

Ronald M. Ueberschaer is a senior research engineer at SRI in the area of radar signal processing. He joined SRI in 1984 after receiving the B.S. degree in physics from Georgia Institute of Technology.

James W. Sinko, a principal engineer at SRI, received the B.S. degree in engineering science and the M.S. degree in electrical engineering from Stanford University, and the Ph.D. degree in electrical engineering from the University of Rochester. Dr. Sinko has worked with radar and aircraft systems at SRI since 1967. For the last 13 years, he has been working with precision GPS for military and civil applications.

Joseph M. Strus is a systems analyst at SRI, where he has worked on precision navigation applications since 2001. His interests are GPS, GPS/INS, and estimation theory, and he holds several GPS-related patents. He received the B.S. and Ph.D. degrees in mathematics from the University of Illinois at Urbana-Champaign. Before coming to SRI he was a GPS systems engineer in the Government Systems Division of Rockwell Collins.

1 ABSTRACT

We report on simulated integration of a tactical grade inertial measurement unit (IMU) with a differential GPS receiver for airborne real-time synthetic aperture radar (SAR) imaging at ultra high frequencies (UHF or P-band). Ten scenarios were investigated for cases simulating characteristics of both differential GPS and IMU errors. Types of errors included 3-D Gaussian position error, Markov random walk errors, simple track offset biases, ramp offsets,

and step-function biases. We confirm previous results that positioning errors affect SAR image formation through an increase in peak and/or integrated sidelobe errors, while biases due to satellite outages and/or IMU integration error affect geolocation accuracy. We conclude that the wavelength is long enough at UHF radar frequencies to enable a tactical grade IMU to be substituted for the navigation grade IMU typically employed in higher frequency microwave SAR systems.

2 INTRODUCTION

In the airborne remote sensing environment, accurate flight track recovery is critical to several parts of the SAR imaging process (Curlander and McDonough, 1991; Carrara *et al.*, 1995). Tracking errors affect image formation as the aircraft flies along the synthetic aperture, as well as geocoding or referencing of the resultant SAR image to an absolute coordinate frame for mapping. For the image formation problem, an airborne UHF SAR requires accurate relative tracking of the airframe position along the entire length of the synthetic aperture, which for a 25° dwell angle producing meter-resolution imagery, is typically on the order of 1–10 km (Figure 1). The tolerable relative positioning error along the synthetic aperture is a fraction of the radar wavelength. For a UHF SAR at 300 MHz carrier frequency, the free-space wavelength is 1 m, resulting in a sub-centimeter relative accuracy requirement for acceptable integrated sidelobe performance.

The long synthetic apertures required for fine-resolution imagery at UHF preclude the use of standard SAR autofocus techniques. In addition, for mapping applications, geocoding of the SAR magnitude imagery to standard coordinate systems such as UTM requires accurate absolute positioning on the order of the achievable SAR resolution, which is typically one meter by one meter at UHF. SRI has been flying low-frequency airborne SAR systems for over 15 years (Vickers *et al.*, 1992), and has demonstrated that dual-frequency L1/L2 GPS post-flight carrier phase differential processing to a reference ground station can support both the SAR imaging and georeferencing requirements. Similarly, real-time on-board differential GPS processing with a StarFire system has provided the neces-

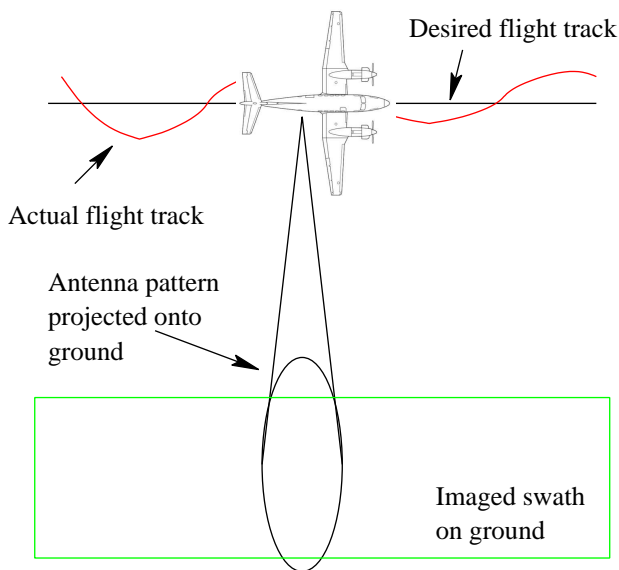


Figure 1. Airborne strip map SAR geometry. True track recovery to a fraction of the free-space radar wavelength is required for proper SAR image formation and geolocation.

sary flight track recovery performance, and enables real-time SAR processing on the aircraft. However, in the airborne kinematic environment, it is not always possible to reliably track the differential correction signal from a single geostationary satellite using an aircraft-roof-mounted antenna. Furthermore, large aircraft roll angles ($> 20 - 25^\circ$) result in a loss of continuous GPS tracking (Navcom Technologies, 2004). In these instances, a viable solution is to combine, in real time, the position solutions from an inertial measurement unit and a differential GPS receiver. SRI has previously developed integrated GPS/IMU solutions for airborne payload tracking applications (Strus *et al.*, 2002).

In this paper we first describe the simulated GPS/IMU system, which employed a real-time differential OmniSTAR receiver and a tactical grade LN-200 IMU. Next we report our findings on studying the effects of various simulated GPS/IMU errors on SAR image quality. We performed this study to assess the applicability of the simulated GPS/IMU system to meet the requirements for SAR image focus and geolocation accuracy.

3 GPS/IMU SYSTEM DESCRIPTION

The GPS/IMU system simulated for this study was the SRI airborne position and location system (APLS) reported previously (Strus *et al.*, 2002). The basic hardware configuration, shown in Figure 2, includes a NovAtel OEM L1/L2 GPS receiver with an OmniSTAR receiver module and XP service subscription, and a Litton LN-200 tactical grade IMU. The extended Kalman filter was chosen as the method of sensor integration. Because of the high-rate nature of the



Figure 2. SRI airborne position and location system (APLS) GPS/IMU package (Strus *et al.*, 2002).

INS data, the navigation processor output is used to provide a reference trajectory for an extended Kalman filter. The filter then processes errors in the system and estimates INS sensor errors. An additional feature in the SRI system is the ability to record raw data for post-processing, which allows us to estimate additional performance criteria. In particular, GPS outages can be added at pre-planned parts of a trajectory. Thus, the “true” error versus the expected error can be measured and used as an additional performance metric for filter tuning.

Two GPS/INS integration schemes are generally considered today. The first is based on feeding the GPS position to the filter (which we call *solution-based*, but which is sometimes called *loosely coupled*). The other scheme feeds individual satellite measurements to the filter (which we call *measurement-based*, but which is sometimes called *tightly coupled*¹). In the solution-based mode, the GPS and INS are treated as separate navigation processes, and the GPS position and/or velocity is used as input to the filter. The GPS position/velocity output is derived either by a separate Kalman filter or by a least-squares algorithm. In the measurement-based mode, the GPS pseudo-range/delta-range and raw INS measurements are inputs into the filter.

For the APLS data processing, the solution-based filter was chosen largely because of its simplicity and independence from the GPS processing task. The initial platform tracking project required a quick integration solution, due to time constraints and the need to consider other applications (Strus *et al.*, 2002). In addition, as work on the filter started, it was not obvious that GPS would provide track-

¹Other authors reserve the term *tightly coupled* for systems in which the IMU measurements are used to control tracking loops in the GPS receiver.

Kalman filter states	Number of states
Position errors	3
Velocity errors	3
Tilt errors	3
Accelerometer bias	3
Gyro bias	3

Table 1. Kalman Filter Parameters

ing data. As such, an independent filter was considered the wisest course. A discussion of the relative merits of the two types of filters appears in (Farrell and Barth, 1999). The GPS receiver was expected to have four or more satellites in view for a large percentage of the tracking period; GPS outage times were not expected to exceed a maximal value of 10 seconds. Furthermore, the correlated noise characteristics of the solution-based filter are somewhat compensated by the longer time allowed for calibration.

There are 15 states in the solution-based Kalman filter, as shown in Table 1. The dynamic error modeling state vector characteristics are similar to the approach of (Farrell and Barth, 1999). The measurement update/gain calculation is computed at every new measurement from the GPS processing task (nominally 10 Hz). The measurement consists of East, North, and Down position errors compensated for lever arm and timing discrepancies between the IMU and GPS. The GPS processing provides the measurements with a standard deviation that is used for the R matrix calculation.

4 POINT TARGET SIMULATIONS

Radar phase history data were generated for a simulated point target, as imaged from an airplane flying a bearing of due north (360°). These phase history data were then processed through SRI's standard time-domain backprojection SAR imaging chain using purposely corrupted tracking data. The effect on image quality was quantified in terms of reduction in the peak sidelobe ratio (PSLR) and increase in the integrated sidelobe ratio (ISLR) metrics (Curlander and McDonough, 1991; Carrara *et al.*, 1995). The ideal azimuthal system impulse response from the unperturbed tracking data, denoted Scenario 0, is shown in Figure 3. This represents a 1-dimensional cut through the 2-D SAR impulse response, taken in the azimuth or along-track direction. This baseline case, denoted Scenario 0 in Table 3, achieved -15.0 dB PSLR and -8.1 dB ISLR².

We investigated ten scenarios for cases simulating characteristics of both differential GPS and IMU errors. Types of errors included 3-D Gaussian position error; Markov random walk errors characteristic of correlated

²All reported ISLR values in this paper are unweighted. Applying a data weighting window or synthetic aperture apodization function can further reduce ISLR (Curlander and McDonough, 1991; Carrara *et al.*, 1995).

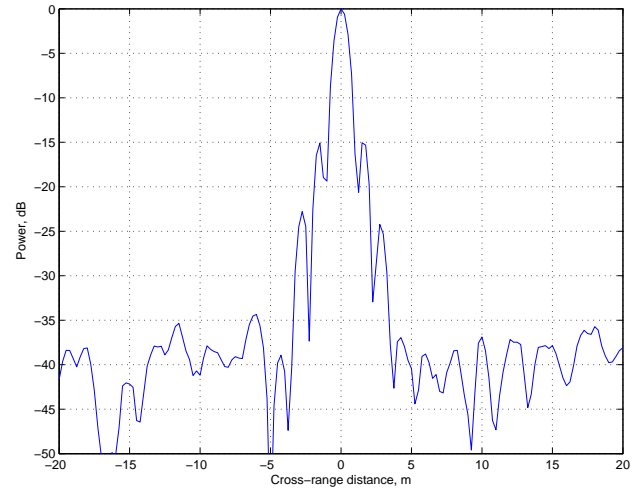


Figure 3. Radar impulse response in the along-track or azimuth dimension, corresponding to Scenario 0 of Table 3 (no perturbations). The achieved SAR resolution is approximately 1 meter at the -3 dB points of the curve. The first sidelobes of the imaging function are at -15 dB, and the integrated sidelobe ratio is -8.1 dB.

Scenario	Parameter 1	Parameter 2
1	$\sigma = 3$ cm	$B = 5$ m
2	$\sigma = 3$ cm	$B = 10$ m
3	$\tau = 2$ s	$\eta = 5$ cm
4	$\tau = 20$ s	$\eta = 15$ cm
5	$a = 20$ cm/s	$b = 0$ m
6	$B_{E,0} = 2.5$ m	$B_{E,1} = -2.5$ m
7	$\sigma = 3$ cm	$B = 0$ m
8	$\sigma = 0$ cm	$B_E = 5$ m
9	$\sigma = 0$ cm	$B_N = 5$ m
10	$\sigma = 0$ cm	$B_U = 5$ m

Table 2. Modeled track perturbations. σ is the standard deviation of a Gaussian random position error. B is a constant bias term, while subscripts E, N, and U denote offsets in the East, North, and Up directions. $B_{E,0}$ and $B_{E,1}$ represent the two limits of a two-state, step-function bias. τ is the time constant of a Markov random walk error, while η is the standard deviation of the driving noise. a is the slope and b the bias of a linear ramp track offset.

noise from a smoothing or carrier filtering receiver; simple track offset biases such as would be caused by either ephemeris or ionospheric/tropospheric model errors; ramp offsets from an improperly integrated IMU initial state; and step-function biases characteristic of loss of view of the satellite constellation without the presence of an IMU. Table 2 summarizes the modeled track perturbations. For parameters that do not contain a specific E, N, or U subscript, the perturbations were applied in all three dimensions.

The effects of the induced errors on the SAR azimuth

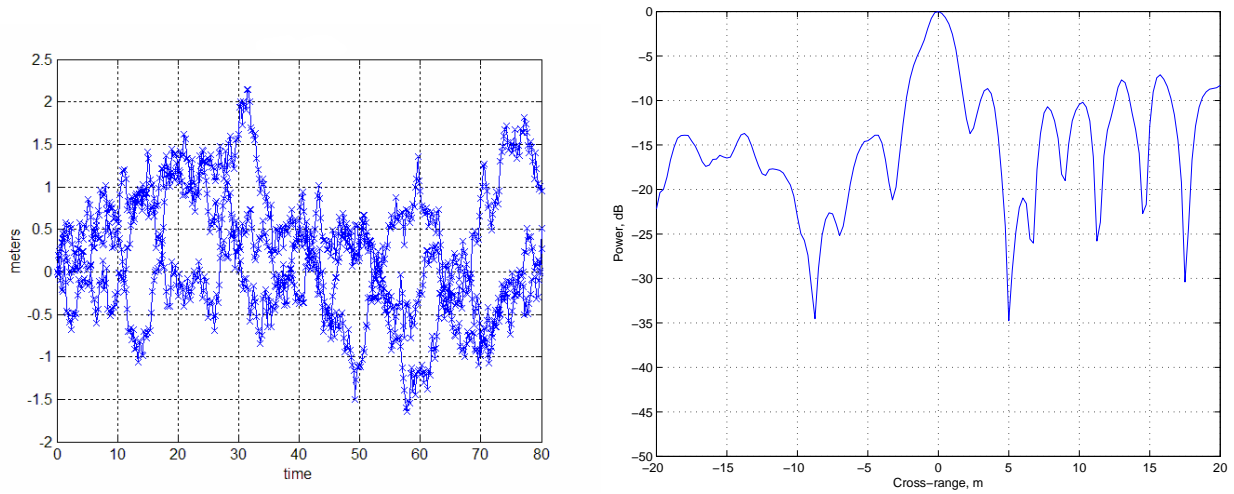


Figure 4. Track position errors in the East, North, and Up directions (left graphic) and SAR azimuth response (right graphic) for Scenario 4 of Table 2. Markov process errors cause blurring and severe reduction of sidelobe performance.

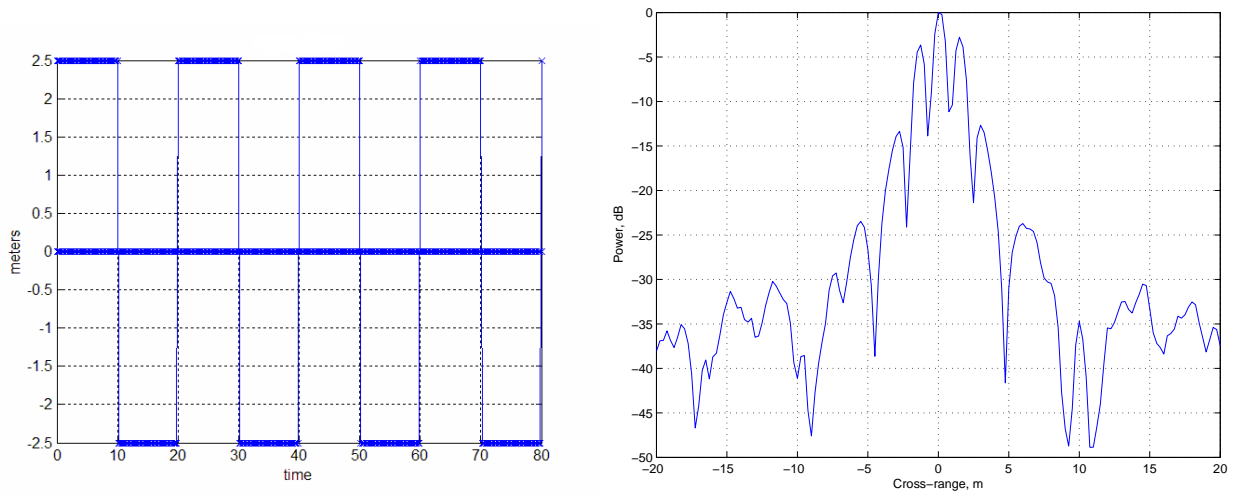


Figure 5. Track position errors in the East, North, and Up directions (left graphic) and SAR azimuth response (right graphic) for Scenario 6 of Table 2. Step-function modulation of the track produces a bifurcation (or “double vision”) and very high first sidelobes in the SAR azimuth response.

Scenario	East, m	North, m	PSLR	ISLR
0	0.0	0.0	-15.0	-8.1
1	+8.2	+1.5	-13.7	-7.9
2	+16.5	+1.0	-10.5	-6.6
3	0.0	-9.0	-5.0	+1.9
4	-0.8	-11.0	-8.5*	+3.6
5	+11.2	0.0	-4.7	+2.4
6	+2.5	+1.4	-2.8**	+0.4
7	0.0	-18.2	-7.6	-4.7
8	+5.0	+0.8	-14.3	-7.4
9	+0.0	+0.8	-12.8	-7.7
10	+3.2	+1.0	-14.2	-7.8

*No well-defined peak

**Bifurcation of peak

Table 3. SAR sidelobe performance. Column 1 gives the scenario number corresponding to the perturbations of Table 2. Columns 2 and 3 report geolocation error of the point target in the East and North directions. Columns 4 and 5 report the measured peak sidelobe ratio (PSLR) and integrated sidelobe ratio (ISLR) in dB (see text).

resolution are depicted in Figures 4 and 5. Table 3 summarizes the quantitative PSLR and ISLR performance.

5 CONCLUSION

We confirmed previous results (Curlander and McDonough, 1991; Muellerschoen and Hensley, 2006) that showed random positioning errors affect SAR image formation through an increase in ISLR, while biases due to satellite outages and/or IMU integration error affect geolocation accuracy. We analyzed discrepancies between the theoretical model for ISLR degradation and geolocation bias versus results from the various perturbations of our simulations. We conclude that at UHF radar frequencies, the wavelength is long enough that a tactical grade IMU can be substituted for the navigation grade IMU typically employed in higher frequency microwave SAR systems. An integrated GPS/IMU sensor with real-time differential corrections enables many SAR applications such as low-sidelobe real-time imaging, repeat-pass incoherent change detection, and repeat-pass SAR interferometry for topographic mapping, deformation monitoring, and coherent change detection.

6 ACKNOWLEDGMENTS

We thank Mr. D.R. Rutt and Dr. W. Graf of the SRI airborne SAR program for many helpful discussions. Funding for this study was provided by the SRI Engineering & Systems Division Independent R&D program, Project #2006-ESD-E4E.

REFERENCES

W.G. Carrara, R.S. Goodman, and R.M. Majewski, *Spotlight Synthetic Aperture Radar*, Artech House, 1995.

J.C. Curlander and R.N. McDonough, *Synthetic Aperture Radar*, Wiley & Sons, 1991.

J.A. Farrell and M. Barth, *The Global Positioning System and Inertial Navigation*, McGraw-Hill, 1999.

R.J. Muellerschoen and S. Hensley, "An evaluation of INU and DGPS measurement fusion for single pass and repeat pass interferometric mapping radars," Proc. ION National Technical Meeting, Monterey, CA 2006.

Navcom Technologies, "VueStar provides Boeing a truth reference for scoring their GPS/INS navigation systems," Project case study, Torrance, CA, 2004.

J.M. Strus, E.G. Blackwell, C.A. Gellrich, M.R. Kirkpatrick, and J.W. Sinko, "Instrumentation of paratroopers and large parachute pallet loads," Proc. ION GPS, Portland, OR, 2002.

R.S. Vickers, V.H. Gonzalez, and R.W. Ficklin, "Results from a VHF impulse synthetic aperture radar," Proc. Conf. Ultrawideband Radar, Los Angeles, CA, 1992.